RF Signal Processing True Time-Delay Beamforming Phased Array

Muhammad Uzair, *Graduate Student Member, IEEE*, Hanxiang Zhang, *Graduate Student Member, IEEE*, Ayesha Naseem, *Student Member, IEEE*, and Bayaner Arigong, *Senior Member, IEEE*

***Abstract*—A true time delay (TTD) beamforming network is proposed from an RF signal processing time-delay block (TDB), which is composed of an RF Hilbert transformer and a tunable transmission line. Here, the RF Hilbert transformer in TDB rotates the electromagnetic waveform by 180° directly in the analog domain without changing its magnitude. To extend the tunable time-delay range, multiple TDBs are cascaded to form a true time-delay network (TDN), realizing the desired time-delay range for a 360° phase change. The theoretical analysis is conducted to explain the RF signal processing TTD and the total time-delay range of TDN. A 1×4 true TDN prototype operating at WiFi frequencies is designed, fabricated, and tested to validate the design concept, and its radiation pattern is measured with integration of a microstrip patch antenna array. The measured beam steering network covers a range of approximately $\pm 45°$ with minimal beam squinting and variation in the gain. All the simulation and measurement results align well with each other to validate the proposed TTD design topology.**

***Index Terms*—RF signal processing, true time delay (TTD), tunable time delay, WiFi phased array.**

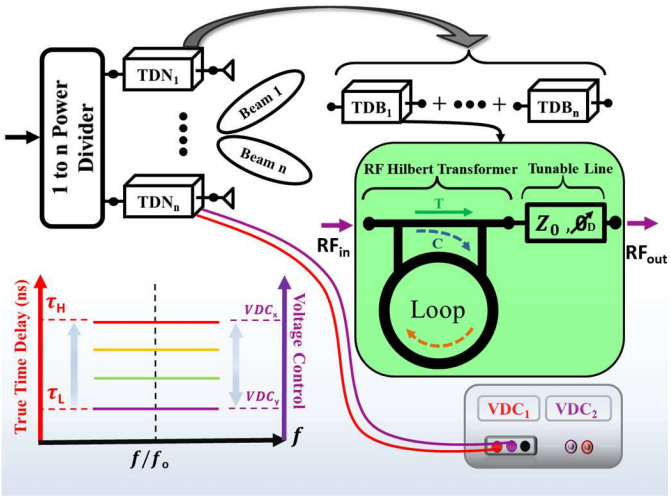

Fig. 1. Proposed tunable TTD phased array feeding network designed from RF signal processing.

I. Introduction

PHASED arrays play important roles in wireless systems to achieve high directivity and gain by controlling the phases and magnitudes of waveforms, and beamforming phased array caters to the need for high data rate transmission and interference management in current 5G/NextG, radar, drone systems, and wireless sensing applications. In emerging wireless technologies, wide instantaneous bandwidths are pursued to support high data throughput and large amount user coverage, which raise many challenges for phase-shifting-based phased array implementation either in digital domain [1], [2], [3], [4] or analog RF domain [5], [6], [7], [8], [9], [10], [11]. Typically, in phase-shifting-phased array design, beam-squinting error and array intersymbol interference are the most critical obstacles for wideband phased array system design using the progressive phase offset method, where the phase shifts depend on frequency variation. To address these issues, true time delay (TTD) phased array is proposed to replace progressive phase delay feeding in antenna arrays, and RF time delay [12], [13], [14], [15], [16], [17], [18], baseband time delay [19], and photonics-aided time delay [20], [21], [22], [23] have been studied to generate frequency-independent radiation pattern without gain loss and distortion in spatial and temporal resolutions.

Different from previous work, in this article, a waveform domain RF signal processing methodology is invented to achieve TTD in a wide frequency band by integrating a coupler-resonator-based Hilbert transformer with a tunable transmission line. This RF signal processing true-time delay network (TDN) is passive, low-loss, continuous, and easy to scale up, which can be applied both in transmitting and receiving channels. As shown in Fig. 1, the proposed TTD beamforming network consists of an RF power divider and true TDNs, and each TDN further contains multiple time-delay blocks (TDBs), which are composed of an RF Hilbert transformer and a tunable transmission line in a cascade manner. Here, the RF Hilbert transformer in each TDB rotates the RF waveform 180° directly in its analog domain without changing its magnitude, and the tunable transmission line allows the tunability of the TTD. The modular design of the TDBs and their integration into TDNs enable their scalability and flexibility, making the system adaptable for a wide range of applications, including high-data-throughput wireless communication, advanced radar systems, and drone systems.

Received 24 July 2025; revised 25 September 2025; accepted 7 October 2025. This work was supported by the National Science Foundation (NSF) under Award ECCS-2340268, Award EES-2230248, and Award CNS-2431438. *(Corresponding author: Bayaner Arigong.)*

The authors are with the Department of Electrical and Computer Engineering, Florida A&M University—Florida State University, Tallahassee, FL 32310 USA (e-mail: barigong@eng.famu.fsu.edu).

Digital Object Identifier 10.1109/TMTT.2025.3620633

In addition, the TDB and TDN are implemented from passive components, allowing the proposed TTD phased array to be either a transmitting array or a receiving array.

This article is presented as follows. First, the theoretical analysis for TDB and TDN is carried out in Section II to determine the time delay in the proposed beamforming phased array. In Section III, a four-channel RF signal processing TTD phased array is designed, fabricated, and validated in simulation and experiment to align with the design concept. By connecting to a patch antenna array, the radiation pattern of the proposed TTD phased array is measured in an antenna chamber, and the measured results show a beam steering range of approximately ±45° with minimal gain variation, validating the effectiveness of the proposed true delay beamforming network. In Section IV, it concludes the proposed design is concluded and discusses future work and potential applications.

II. Design Theory of RF Signal Processing True TDN

As in Fig. 1, our proposed tunable TDN is designed from an RF signal processing tunable TDB, which is composed of an RF Hilbert transformer and a tunable delay line. Based on the phase response of TDB, multiple TDBs are cascaded to realize a large tunable time-delay range across the wide frequency band, and two-channel control voltages are applied to continuously configure the time delay, achieving a wide beam scanning angle.

A. Time Delay of RF Signal Processing True TDN

As shown in Fig. 2, the RF Hilbert transformer is a key component in TDB, which is designed using a rat-race coupler and resonating feedback transmission line as discussed in [24] and [25]. From signal flow analysis as shown in Fig. 2(a) and (b), the transfer function of the coupler-resonator-based Hilbert transformer can be derived as

$$S_{\mathrm{HBT}_{21}} = S_{21} + \frac{S_{31} S_{\mathrm{loop}} S_{24}}{1 - S_{34} S_{\mathrm{loop}}}. \tag{1}$$

Fig. 2(c) shows the explanation of the signal flow analysis in each branch. In the first step, the feedback loop is simplified, which forms a series connection with S_{31} and S_{24}. The equivalent circuit then forms a parallel connection with the S_{21}. The phase introduced by the lossless transmission can be substituted as $e^{-j\theta}$ in (1). The finalized transfer function in (2) can be used to calculate the total phase rotation of the coupler-resonator-based RF Hilbert transformer, given by (3)

$$S_{\mathrm{HBT}_{21}} = e^{-j\theta_{21}} + \frac{e^{-j\theta_{31}} e^{-j\theta_{\mathrm{loop}}} e^{-j\theta_{24}}}{1 - e^{-j\theta_{34}} e^{-j\theta_{\mathrm{loop}}}} \tag{2}$$

$$\varphi_{\mathrm{HBT}_{21}} = \angle \left\{ S_{\mathrm{HBT}_{21}} \right\}. \tag{3}$$

In order to tune the phase of RF Hilbert transformer, a tunable delay line is cascaded with Hilbert transfer as shown in Fig. 3. The tunable delay line (Z_0, θ_D) in Fig. 3 is implemented by cascading two identical transmission line sections $(Z_\alpha, \theta_\alpha)$ in series along with three short-ended shunt varactors at input, output, and center, respectively [26], which are denoted as C_1

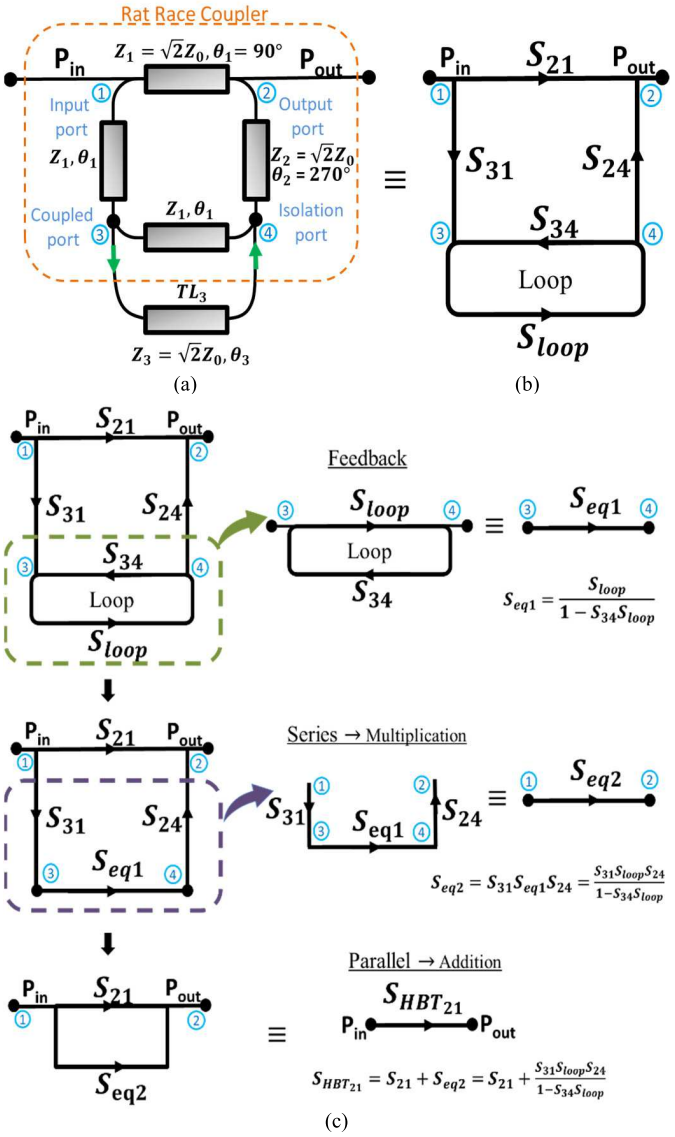

Fig. 2. (a) Transmission line RF Hilbert transformer circuit. (b) Signal flowchart of the RF Hilbert transformer. (c) Detailed signal flow analysis of the RF Hilbert Transformer.

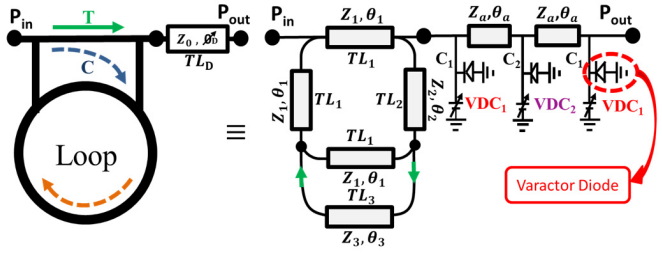

Fig. 3. Schematic of tunable TDB.

and C_2 in Fig. 3. From the analysis, the ABCD matrix of the tunable line is derived by cascading the ABCD matrix of the shunt capacitors and series transmission line given by following equations:

$$\begin{pmatrix} A_{C_1,C_2} & B_{C_1,C_2} \\ C_{C_1,C_2} & D_{C_1,C_2} \end{pmatrix} = \begin{pmatrix} 1 & 0 \\ j\omega C_{1,2} & 1 \end{pmatrix} \tag{4}$$

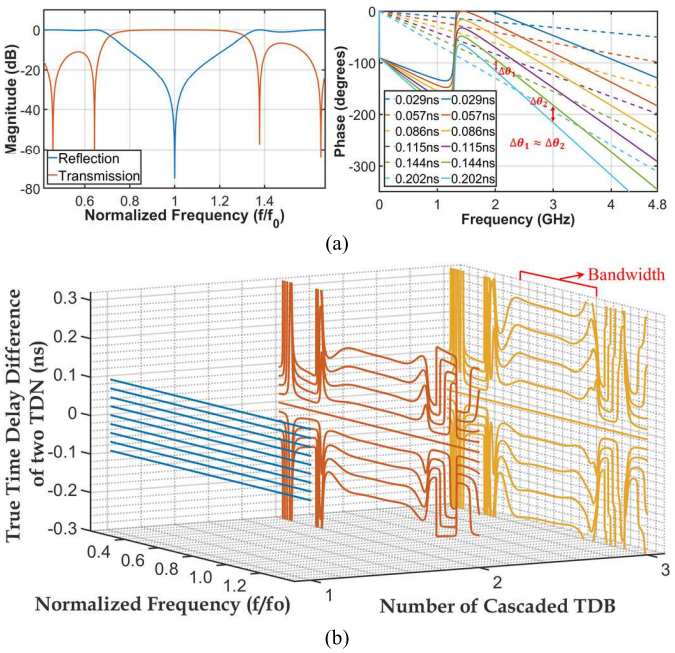

Fig. 4. Tunable time delay from RF signal processing. (a) Frequency and phase response of ideal TDB. (b) Tunable time delay difference range of TDN with difference cascaded TDBs.

$$\begin{pmatrix} A_L & B_L \\ C_L & D_L \end{pmatrix} = \begin{pmatrix} \cos\theta_a & jZ_a \sin\theta_a \\ jY_a \sin\theta_a & \cos\theta_a \end{pmatrix} \tag{5}$$

where Z_a and θ_a are the characteristic impedance and the electrical length of the transmission line between the shunt capacitors

$$\begin{aligned} \begin{pmatrix} A_{\mathrm{TL}} & B_{\mathrm{TL}} \\ C_{\mathrm{TL}} & D_{\mathrm{TL}} \end{pmatrix} &= \begin{pmatrix} 1 & 0 \\ j\omega C_1 & 1 \end{pmatrix} \begin{pmatrix} \cos\theta_a & jZ_a \sin\theta_a \\ jY_a \sin\theta_a & \cos\theta_a \end{pmatrix} \\ &\times \begin{pmatrix} 1 & 0 \\ j\omega C_2 & 1 \end{pmatrix} \begin{pmatrix} \cos\theta_a & jZ_a \sin\theta_a \\ jY_a \sin\theta_a & \cos\theta_a \end{pmatrix} \\ &\times \begin{pmatrix} 1 & 0 \\ j\omega C_1 & 1 \end{pmatrix}. \end{aligned} \tag{6}$$

By matrix multiplication, $A_{\mathrm{TL}}, B_{\mathrm{TL}}, C_{\mathrm{TL}}$, and D_{TL} are given in the following equations, (7)–(10), respectively,

$$\begin{aligned} A_{\mathrm{TL}} &= \cos 2\theta_a - 0.5 \sin 2\theta_a \left(2\omega Z_a C_1 + \omega Z_a C_2\right) \\ &\quad + \omega^2 C_1 C_2 Z_a^2 \sin^2\theta_a \end{aligned} \tag{7}$$

$$B_{\mathrm{TL}} = jZ \sin 2\theta_a - j\omega C_2 Z_a^2 \sin^2\theta_a \tag{8}$$

$$\begin{aligned} C_{\mathrm{TL}} &= j\omega C_1 \cos 2\theta_a + \frac{j \sin 2\theta_a}{Z_a} + j\omega \left(C_1 + C_2\right) \cos^2\theta_a \\ &\quad + j\omega C_1 \times \left(C_1 C_2 \omega^2 Z^2 - 1\right) \sin^2\theta_a \\ &\quad - j0.5\omega^2 Z_a \left(2C_1^2 + C_1 C_2 + C_2\right) \sin 2\theta_a \end{aligned} \tag{9}$$

$$D_{\mathrm{TL}} = A_{\mathrm{TL}}. \tag{10}$$

From the *ABCD* parameter, we get the S_{21} of the tunable line as

$$S_{\mathrm{TL}_{21}} = \frac{2}{A_{\mathrm{TL}} + \frac{B_{\mathrm{TL}}}{Z_o} + C_{\mathrm{TL}} Z_o + D_{\mathrm{TL}}} \tag{11}$$

$$\varphi_{\mathrm{TL}_{21}} = \angle \left\{ S_{\mathrm{TL}_{21}} \right\}. \tag{12}$$

The total time delay introduced by each TDB can be calculated using the time delay of the RF Hilbert transformer and tunable transmission line in cascade, which is derived in (13). By controlling the capacitance ranges of two diodes, the time delay can be tuned

$$T_{\mathrm{TDB}} = \left(\frac{\varphi_{\mathrm{HBT}_{21}}}{360 \times f}\right) + \left(\frac{\varphi_{\mathrm{TL}_{21}}}{360 \times f}\right) \tag{13}$$

where $\varphi_{\mathrm{HBT}_{21}}$ and $\varphi_{\mathrm{TL}_{21}}$ are the phase responses of the Hilbert transformer and tunable delay line, respectively, and f is the operating frequency. Fig. 4(a) (left) shows the transmission and reflection response, where the horizontal axis is normalized by the center operating frequency f_0, and Fig. 4(a) (right) shows the phase response of the ideal TDB and the transmission line with different time delays. The phase response of ideal transmission lines with different time delays shows different slopes as plotted in a dashed line in Fig. 4(a) (right). The phase response of TDB with different time delays shows the same slope with a constant offset across the frequency band, realizing a frequency-independent TTD characteristic. Fig. 4(b) shows the time delay difference between the two tunable TDN plotted across the frequency band. Here, the negative time delay indicates that the second TDB heads up from the first TDB. As shown in different line plots in Fig. 4(b), the range of single tunable TDB is about ±0.07 ns, which is about ±60° progressive phase difference between two TDB at the operating frequency of 2.4 GHz. To extend the tuning range of tunable time delay, multiple TDBs are cascaded to form TDN. As shown in Fig. 4(b), cascading two and three TDB, the tunable time delay difference range can reach to range of ±0.14 and ±0.21 ns, respectively. At the same time, it is observed that the bandwidth of TDN is smaller for a large number of cascaded TDBs. From Fig. 4(b), it is clear that the tradeoff between time-delay range and bandwidth is a key design parameter for practical design. The bandwidth is mainly limited by the transmission line implementation of RF signal processing TDB, especially with a rat-race coupler and resonating transmission line feedback. To expand the frequency bandwidth, a wideband rat-race coupler can be designed and integrated into an RF Hilbert transformer, which can be further discussed in future work.

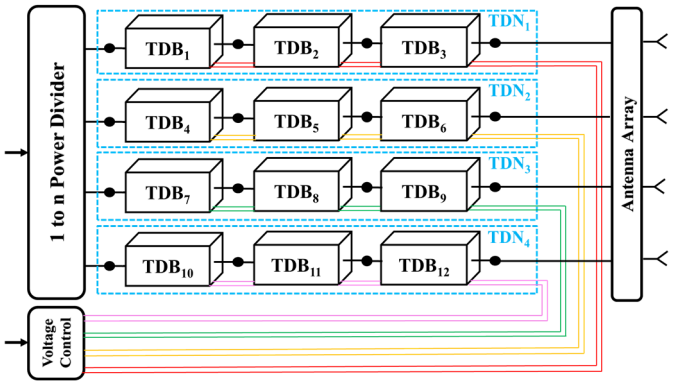

Fig. 5. Schematic of 1 × 4 True TDN.

B. 1 × 4 *True TDN Design*

With the analysis of TDB and TDN, a 1 × 4 RF signal processing true TDN is designed from four TDN networks,

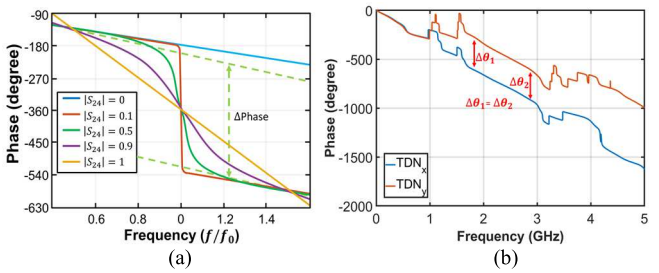

Fig. 6. (a) RF Hilbert transformer response at different coupling coefficient magnitudes $|S_{24}|$, where f_0 is the normalized center frequency. (b) Simulated phase response of the True TDNs.

where each TDN is further composed of three true-TDBs as shown in Fig. 5. The Hilbert transformer in TDB and TDN processes the signal directly in the waveform domain to enable phase response slope adjustment, realizing a constant phase offset between two TDNs in a wide frequency range. Fig. 6(a) shows that the transmission line-based Hilbert transformer processes the RF signal to achieve its phase rotation by controlling the coupling coefficient $|S_{24}|$ in (1). Fig. 6(b) shows the phase responses of two TDNs for a center frequency of 2.4 GHz, where the constant offset ($\Delta\theta_1 = \Delta\theta_2$) phase between two TDNs across the band enables TTD in a wide frequency range. This offset can be controlled and tuned by using the tunable transmission lines in TDNs. The output from each TDN is fed into the antenna array, and the time delay in each channel is electronically controlled using an external dual-voltage supply. The total time delay (T_{total}) for each TDN chain is the sum of the delays introduced by the individual TDBs within that channel, given by the following equation, where the T_{TDBj} is the time delay introduced by each TDB:

$$T_{\text{total}} = \text{TDB}_1 + \text{TDB}_2 + \text{TDB}_3 \tag{14}$$

$$T_{\text{TDN}_i} = \sum_{j=3i-2}^{3i} \text{TDB}_j, \quad (i = 1, 2, 3, 4). \tag{15}$$

III. Implementation of Proposed True TDN

A. True TDN Measurements

To validate our design concept, a four-channel TTD phase array feeding network is designed from the proposed TDN, where each channel contains three cascaded TDBs, realizing ±0.21-ns tunable time delay for a full beam steering angle of ±45° at 2.4 GHz. The schematic of the four-channel TDN prototype and its design parameters are shown in Fig. 7(a). Here, $Z_1, Z_2, Z_3, \theta_1, \theta_2$, and θ_3 represent the impedances and electrical lengths of the transmission lines in the RF Hilbert transformer. Similarly, Z_a and θ_a represent characteristic impedance and the electrical length of the transmission line between two varactors in a tunable transmission line. The design values for transmission lines and lumped elements are given in Fig. 7(a). The circuit is fabricated on RO4350B substrate ($\varepsilon_r = 3.66, \tan\delta = 0.0031$) with a thickness of 0.51 mm and copper cladding of 35 μm. The prototype is shown in Fig. 7(b), and the size of the fabricated circuit is 137 × 125 mm. The varactor diodes MA46H120 are used to tune the capacitances in (6) and, consequently, the phase of the tunable delay line. RF chokes and dc blocks are designed to bias

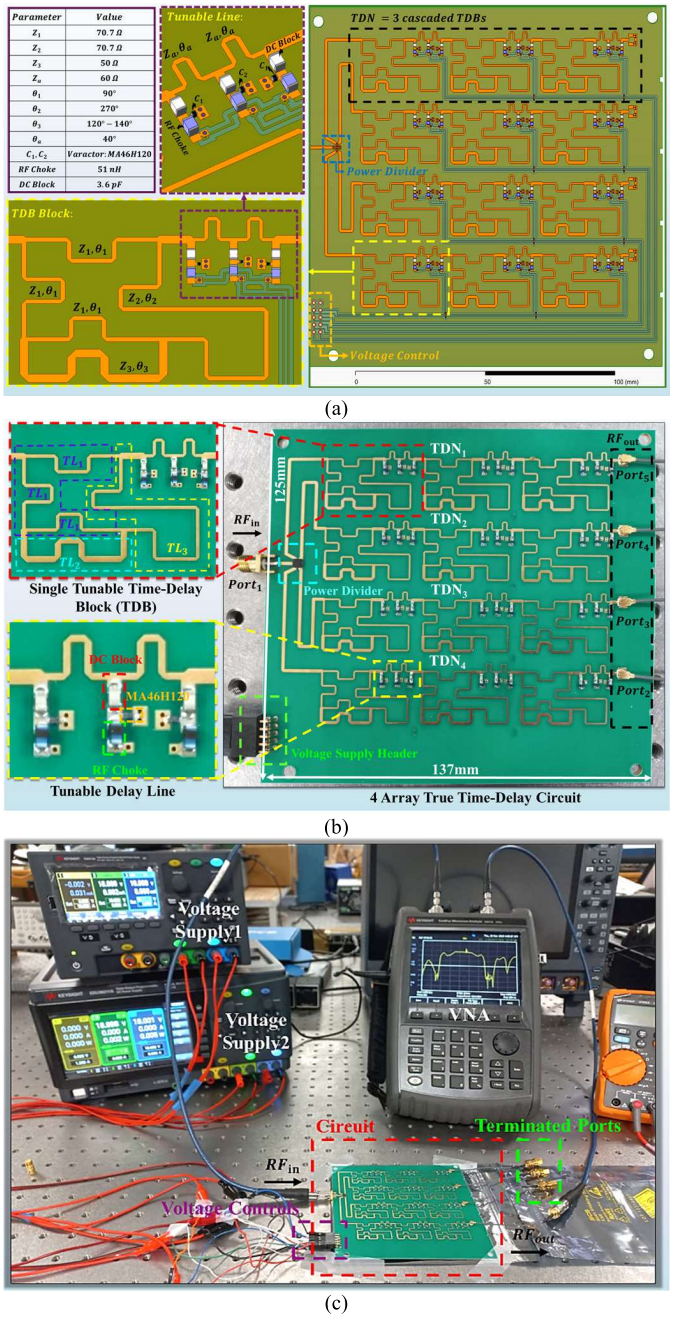

Fig. 7. Experiment validation of the proposed RF signal processing true time-delay array. (a) Prototype model and design parameters. (b) Fabricated a prototype of a four-channel TDN. (c) Experimental setup for validation of the prototype.

the varactors. A four-way power splitter (WP4U+) is used at the input port to split the RF signal equally among all four tunable TDN chains. The input signal is fed through the subminiature version (SMA) connector, and the outputs are transferred through ultraminiature coaxial connector (UFL) connectors to the antenna array.

The four tracks after the power splitter are phase-matched to ensure each channel has equal phase at the input of TDN. Fig. 7(c) shows the experiment setup, where the circuit is connected to a dc voltage supply for controlling the varactor diode, and the frequency response is measured using a Keysight FieldFox vector network analyzer. The EM simulation and

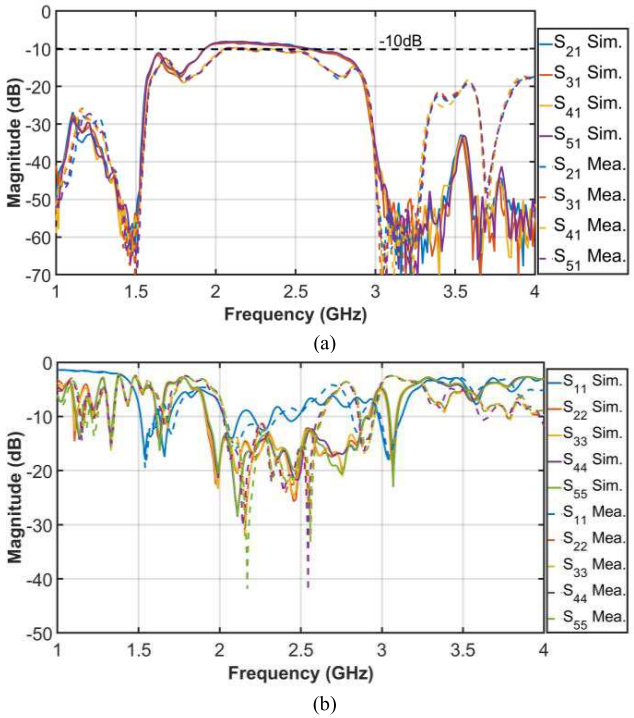

Fig. 8. Simulated and measured results of the proposed true time-delay array. (a) Magnitude response of transmission. (b) Magnitude response of return loss.

measurement results are summarized in Fig. 8. Specifically, Fig. 8(a) presents the transmission of each TDN, with port names indicated in Fig. 7(b). The simulated transmissions are plotted in a solid line, and the measured transmissions are plotted in a dashed line. The overall in-band transmission loss is around 9 dB, including approximately 6.5-dB loss from the four-way power divider. The return losses are better than 10 dB across the frequency band, as shown in Fig. 8(b). A slightly higher insertion loss observed in the measured response is primarily attributed to the output subminiature push-on (SMP)-to-SMA cable losses. In addition, Fig. 9(a) shows the time delay difference between TDN_2 with reference to TDN_1. The time-delay response is obtained with a step of 60° at the operating frequency of 2.4 GHz. The negative time delay indicates that the delay is introduced in the TDN_2 relative to the first. Similarly, Fig. 9(b) and (c) shows the time delay difference of TDN_3 and TDN_4 with reference to TDN_1, respectively. Slight distortions in time-delay response are primarily attributed to modeling accuracy, fabrication tolerances, and the laboratory assembling process of surface mount components with a small pad size. Additional contributions come from measurement tolerances, especially in the junction of the UFL to the SMA connector.

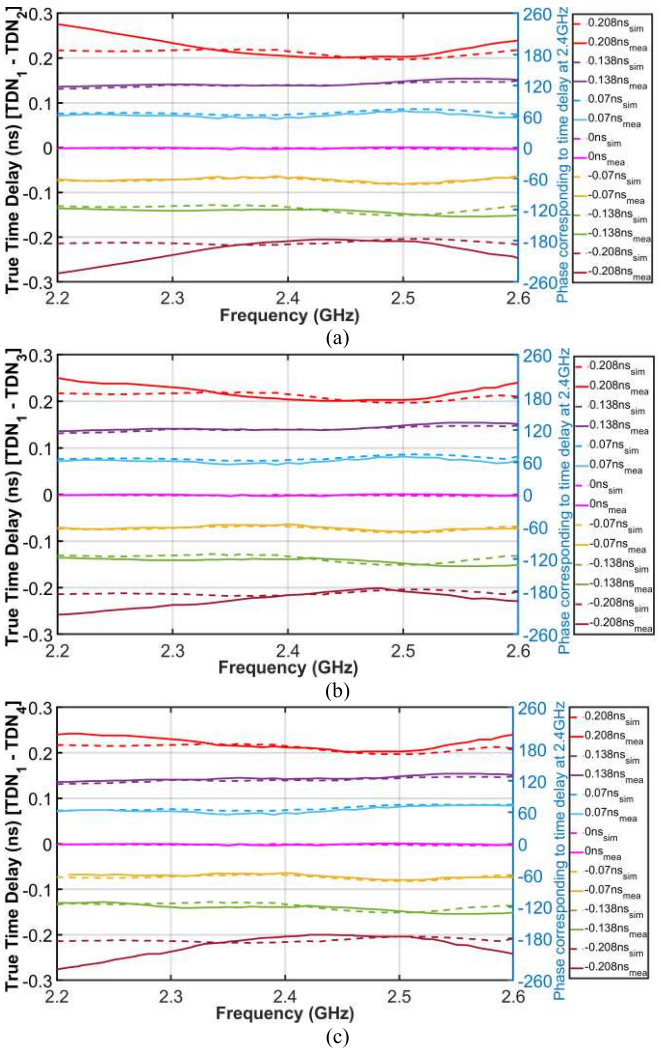

Fig. 9. Tunable time-delay response across the frequency band of (a) TDN_2, (b) TDN_3, (c) TDN_4.

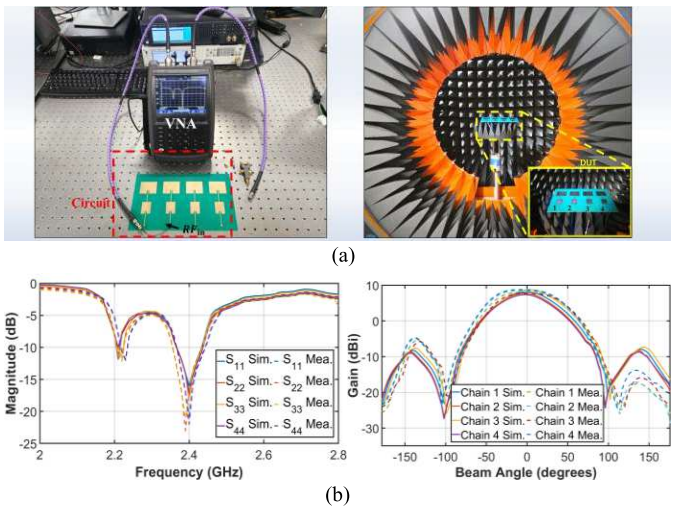

Fig. 10. Measurement setup and results. (a) Measurement setup for antenna return loss and radiation pattern. (b) Antenna return loss results (left). Antenna radiation pattern results (right).

B. Radiation Pattern Measurements

The TTD achieved at the output of four channels of the TTD circuit is fed into a 4×1 microstrip patch antenna array through UFL–UFL cables to measure the radiation pattern for beamforming application. Each antenna element in the array consists of two series-fed microstrip patches, where the patch widths and inset feed are adjusted to match 50 Ω. The spacing between antenna elements is $\lambda/2$ at the center frequency. Fig. 10 shows the experiment setup and measured

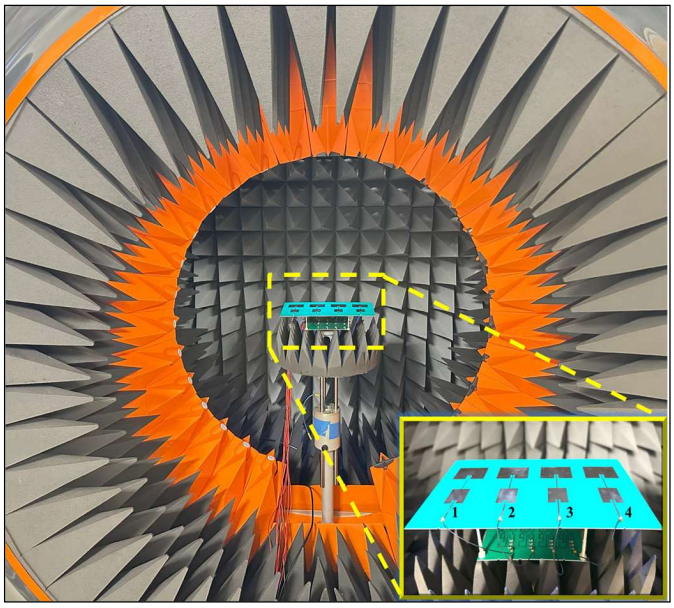

Fig. 11. Experimental setup for the radiation pattern measurement.

TABLE I

BEAMFORMING ANGLE AND THE CORRESPONDING VOLTAGES AT EACH TDN

Beamforming Angle	Progressive Phase Difference Applied to Array	TDN_1		TDN_2		TDN_3		TDN_4	
		V_A	V_B	V_C	V_D	V_E	V_F	V_G	V_H
-40	-180	19	19	12	12	6	6	1	1
-30	-135	16	16	8	8	5	5	1	1
-20	-90	14	14	9	9	4.5	4.5	1	1
-10	-45	10	10	7	7	4	4	2	2
0	0	10	10	10	10	10	10	10	10
10	45	2	2	4	4	7	7	10	10
20	90	1	1	4.5	4.5	9	9	14	14
30	135	1	1	5	5	8	8	16	16
40	180	1	1	6	6	12	12	19	19

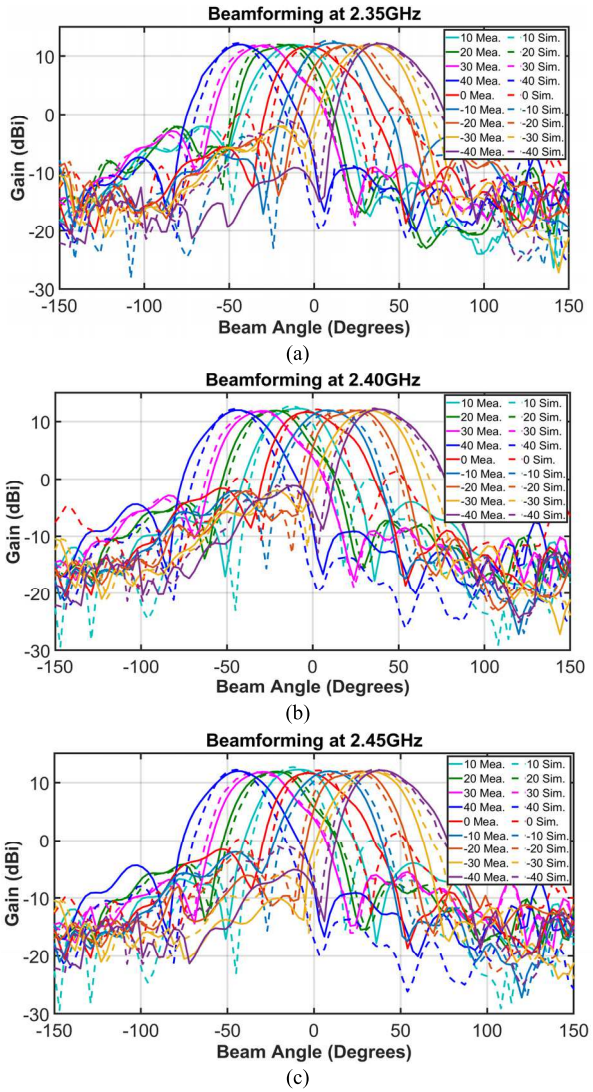

Fig. 12. Experiment validation of the beamforming circuit. (a) Radiation pattern measurements at 2.35, (b) 2.40, and (c) 2.45 GHz.

results of the antenna element in the phased array. Specifically, Fig. 10(a) shows the experimental setup for the return loss and the radiation pattern measurements. Fig. 10(b) (left) shows the simulated and measured return loss of each antenna, which is less than 10 dB across the operating band, and Fig. 10(b) (right) plots the simulated and measured radiation patterns of each antenna element in the array, showing a gain of approximately 7.8 dBi. The antenna array is fabricated on RO4350B substrate ($\varepsilon_r = 3.66, \tan\delta = 0.0031$) with a thickness of 0.76 mm and copper cladding of 35 μm. The size of the antenna array is 150×260 mm. The designed antenna array has a gain of approximately 13.1 dBi at the operating frequency of 2.4 GHz. Fig. 11 shows the experimental setup using the MVG Starlab anechoic chamber for measurement of the radiation pattern. The measurement setup shows the antenna PCB at the top and the TTD PCB at the bottom assembled through plastic screws. The TTD PCB is connected to Keysight dc power supplies E36313A to control TTD and the beam angle. Table I shows the beamforming angles and their corresponding control voltages.

The measured radiation pattern from the anechoic chamber is post-processed in MVG Wave studio, and the data is plotted on MATLAB as shown in Fig. 12(a)–(c). The figures present a comparison between the measured and simulated results of gain versus beam angle. Fig. 12(a)–(c) shows the test results at frequencies 2.35, 2.4, and 2.45 GHz, respectively, to validate the TTD concept and confirm the minimal variation in beam direction with frequency, confirming the frequency-independent steering performance. The central beam corresponds to a beam angle of 0° when equal voltages are applied to all four chains. To steer the beam, the voltages are varied between 1 and 19 V. Different combinations of voltages and beam angles are given in Table I. As per the results, the measured data show agreement with the simulated data, validating the design theory of TTD, where the radiation pattern and beam angle are approximately the same in the frequency band.

C. Modulated Signal Measurements for WiFi Application

To evaluate the system-level performance of the proposed true TDN, the error vector magnitude (EVM) and I/Q con-

TABLE II
COMPARISON BETWEEN EXISTING TRUE TDNS

Item	Ref. [14]	Ref. [15]	Ref. [16]	Ref [17]	Ref [18]	Ours
Topology	gm-C Cascaded Analog All-Pass	Switched Constant R network	All-Pass Filter-Based Delay Cell	CPW + Varactor-Based Delay Module	Three-Layer Tree Delay Network	Hilbert Transformer + Tunable Line
Fabrication Process	160nm CMOS IC	GaAs MMIC	180nm CMOS	Thin Film CPW	Multilayer RF PCB	RF PCB Standard Etched
Frequency	1-2.5 GHz	2-4GHz	5 GHz	8–12 GHz	27–33 GHz	2.35-2.45GHz
Delay Range	550 ps (40×13 ps)	5-155 ps (5 bits × 5 ps)	~60 ps	Quantized 6-bit range	Configurable mmWave delays	80ps per TDB (Cascadable)
Insertion Loss	<1.8 dB	<8 dB	Not specified	< 1 dB	Moderate	<1dB
Tunability	digitally controllable delay steps	Not specified	Low - Not modular	Medium - Quantized Levels	Medium - Modular tree structure	Continuous voltage-controlled
Scalability / Modularity	High – Cascadable	Medium – Bit-scalable	Active analog delay in compact CMOS	Thin CPW + varactor-based 6-bit switchable delay	Compact three-layer analog TTD network	High-Cascadable Delay Blocks
Distinct Feature	High-resolution analog tuning	High-resolution delay (5 ps) for SIC	All-Pass Filter-Based Delay Cell	CPW + Varactor-Based Delay Module	Three-Layer Tree Delay Network	Passive RF, low loss, scalable delay, RF PCB
Beam steering	±60°	Not reported	Not reported	Not reported	±34°	±45°
Array Gain	Not reported	Not reported	Not reported	Not reported	Not reported	13.1dBi
EVM	Not reported	Not reported	Not reported	Not reported	Not reported	3–4% (16-/64-/256-QAM)

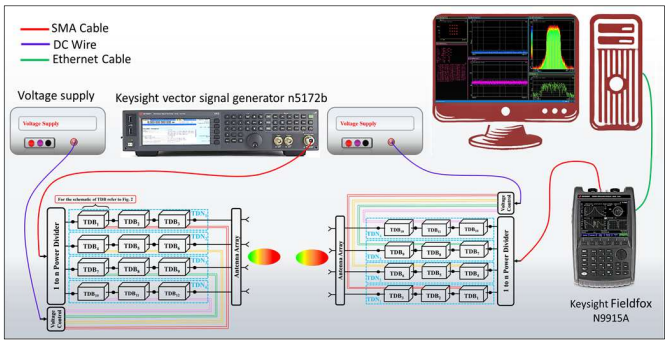

(a)

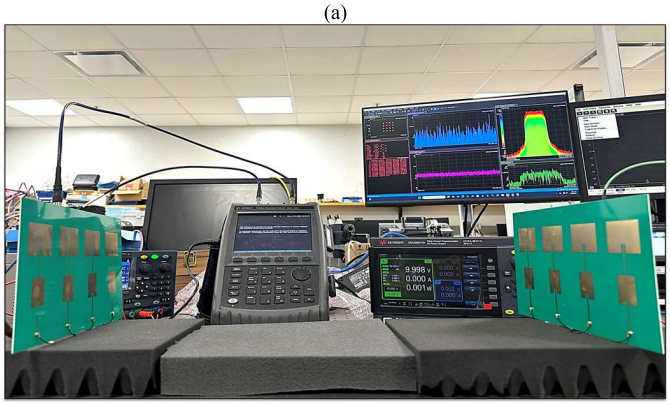

(b)

Fig. 13. Measurement setup. (a) Test setup connections. (b) Experimental setup.

stellation measurements are performed. These experiments are particularly important for WiFi and 5G/NextG applications, where higher-order modulation schemes require high linearity with less signal distortion. The signal quality transmitted through the proposed system is examined under different operating frequencies and beam steering conditions to validate its suitability for practical wireless communication scenarios. Fig. 13 shows the measurement setup for the modulated signal applied to the proposed TTD phased array. The I/Q modulated signal is generated using a Keysight N5172B signal generator, fed into the true TDN, and radiated through the antenna array. The radiated signal is received by another antenna array and passed through the TDN to a Keysight FieldFox network analyzer. FieldFox is connected to the VSA software on a PC via Ethernet. The received signal is measured, and the I/Q constellation results for different modulated signals are shown in Figs. 14 and 15, where the measured EVM is approximately 4.1% for 64-quadrature amplitude modulation (QAM) and 3.2% for 256-QAM, demonstrating reliable modulation accuracy even for higher-order constellations. Fig. 14 shows the impact of beam steering for signal quality at a fixed frequency of 2.4 GHz for three modulation types: 16-QAM, 64-QAM, and 256-QAM. For 16-QAM as shown in Fig. 14(a), the constellation points are well-defined and retain a square structure across all tested beam angles (±40°, ±20°, and 0°), showing an EVM of 4.3%. For 64-QAM as shown in Fig. 14(b) and 256-QAM as in Fig. 14(c), some dispersion appears at large steering angles, but the constellation remains structured with an EVM of 4.1% and 3.2%, respectively, suggesting a modest degradation in signal quality due to increased angular offsets. Fig. 15 presents the effect of operating frequency on the constellation at a

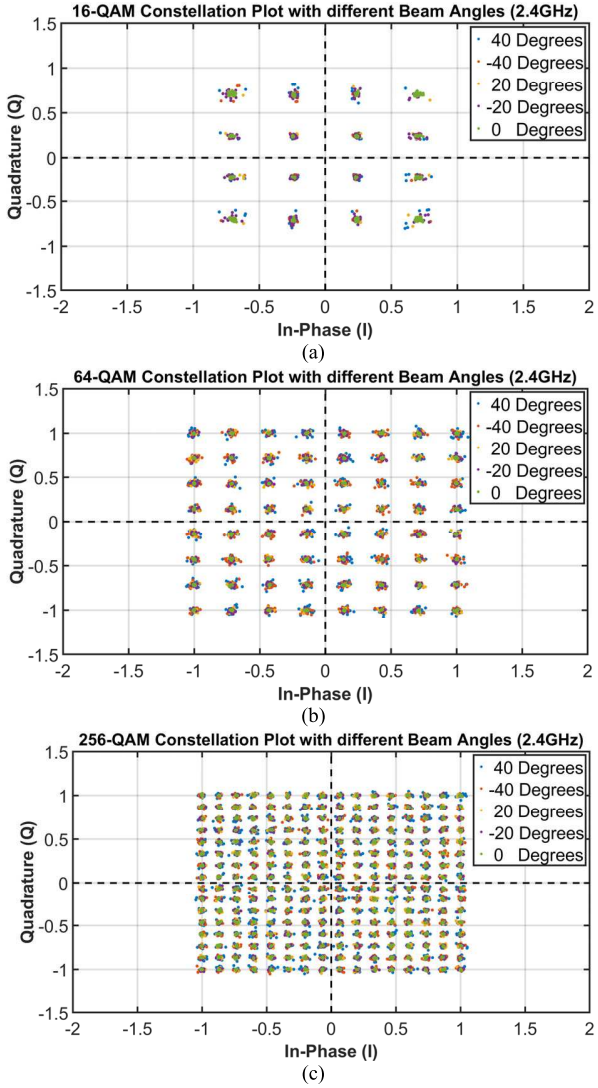

Fig. 14. Constellation measurement results at different beam angles: (a) 16-QAM, (b) 64-QAM, and (c) 256-QAM.

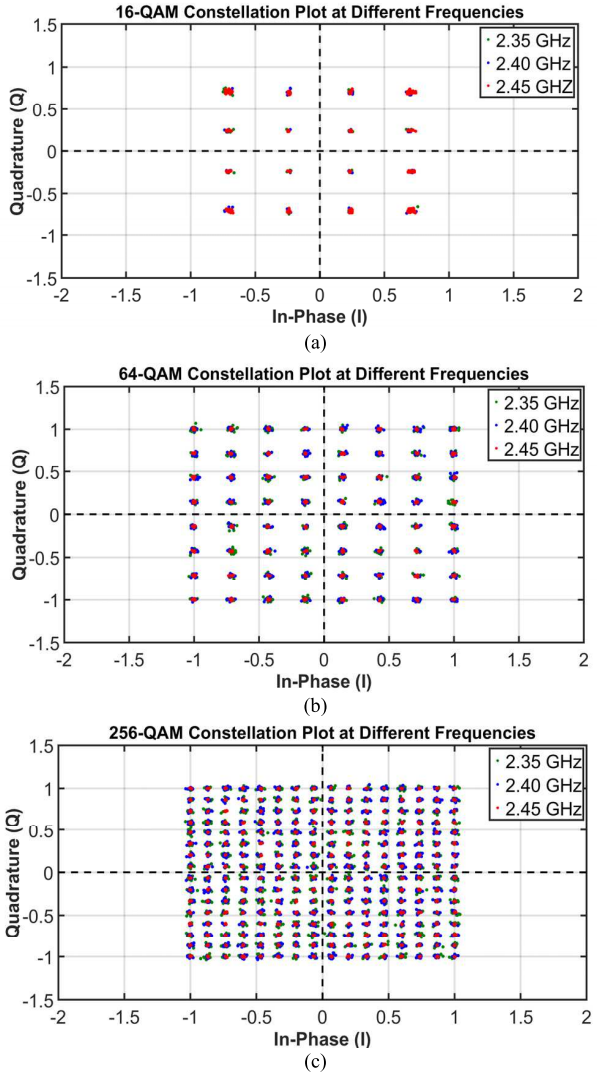

Fig. 15. Constellation measurement results at different frequencies: (a) 16-QAM, (b) 64-QAM, and (c) 256-QAM.

fixed beam direction, tested at 2.35, 2.40, and 2.45 GHz. For 16-QAM as shown in Fig. 15(a), the constellation remains gathered with EVM of 3.7% across the entire frequency range, implying frequency stability of the proposed design. For 64-QAM as in Fig. 15(b), and 256-QAM as in Fig. 15(c), slight spreading is noticeable with EVM of around 3.9% and 3.1%, respectively. The EVM measurement of the proposed TTD phased array system has a small degradation, which is mainly caused by the insertion loss of passive TDN, ripples from cascaded tunable transmission line sections, and varactor nonlinearity. The degradation can be further improved by reducing insertion loss and return loss, and an additional calibration process. Overall, the measurement results confirm that the system sustains reliable performance across varying beam angles and frequency shifts, making it suitable for TTD applications with minimal beam squinting and signal distortion.

Table II compares the proposed TTD network with the state-of-the-art designs, which includes system topology, fabrication process, operating frequency, achievable delay range, insertion loss, tunability, and scalability. Our design employs a passive Hilbert transformer cascaded with a tunable transmission line implemented on a standard RF PCB, offering continuous delay control over the 2.35–2.45 GHz band with a compact and scalable architecture. The use of passive circuitry not only ensures low insertion loss (<1 dB) but also enables bidirectional operation, making the network suitable for both transmit and receive paths. Unlike gm-C and all-pass CMOS implementations [14], [16], which offer limited tunability and are confined to integrated environments, the bit-switched GaAs MMIC in [15] provides excellent resolution but limited scalability. Compared with varactor-loaded and tree-structured delay lines [17] and [18], which target higher frequencies with discrete tuning levels, our approach provides fine-grain analog tunability suitable for low-cost transmitting and receiving RF systems. Overall, our proposed RF signal processing true TDN is a compelling candidate for practical, low-cost, and low-loss TTD phased-array beamforming applications.

IV. Conclusion

In this article, a TTD beamforming feeding network is designed from an RF signal processing TDB, which is composed of a coupler-resonator-based RF Hilbert transformer and an electronically tunable transmission line. The proposed TDN can be tuned in a range of ± 0.21 ns difference at the operating frequency of 2.4 GHz, covering a phase angle of $\pm 180°$. To validate the design theory, a prototype is designed, fabricated, and validated in the experiment for low-cost beam-squinting free WiFi beamforming applications. The modulated signals are applied in transmission and receiving modes of the proposed passive true TDN to verify the linearity of the proposed design. Overall, the measurement results align well with the design theory and simulations to validate the proposed RF signal processing-based TTD phased array concept. In our future work, the TTD will be implemented in the MMIC to further miniaturize the size. In addition, a fully integrated 3-D true-time delay phased array will be designed and fabricated using a 3-D printer for drone-based applications. Expanding the bandwidth of the Hilbert transformer and proposing true TDN are also planned to enhance overall system performance for wideband applications.

References

[1] B. Hu, P. Chen, J. Xu, and X. Yu, "Low-cost digital phase-shifting technique using delta-sigma modulation for satellite communication antenna systems," *IEEE Trans. Microw. Theory Techn.*, vol. 71, no. 2, pp. 842–853, Feb. 2023.

[2] C. Fulton, M. Yeary, D. Thompson, J. Lake, and A. Mitchell, "Digital phased arrays: Challenges and opportunities," *Proc. IEEE*, vol. 104, no. 3, pp. 487–503, Mar. 2016.

[3] S. Jang, R. Lu, J. Jeong, and M. P. Flynn, "A 1-GHz 16-element four-beam true-time-delay digital beamformer," *IEEE J. Solid-State Circuits*, vol. 54, no. 5, pp. 1304–1314, May 2019.

[4] F. Liu, J. Xu, Y.-W. Duan, H. Wan, H. Zhang, and L. Zhu, "A 5-bit digital phase shifter using phase-tuning property of open-/short-circuit microstrip line-loaded slot line structure," *IEEE Trans. Microw. Theory Techn.*, vol. 71, no. 6, pp. 2606–2615, Jun. 2023.

[5] H. Zhang, H. Ren, P. Liu, H. Yan, and B. Arigong, "Tunable 3 × 3 nolen matrix network for power-saving phased array," *IEEE Microw. Wireless Technol. Lett.*, vol. 34, no. 8, pp. 995–998, Aug. 2024.

[6] H. Ren, P. Li, Y. Gu, and B. Arigong, "Phase shifter-relaxed and control-relaxed continuous steering multiple beamforming 4 × 4 Butler matrix phased array," *IEEE Trans. Circuits Syst. I, Reg. Papers*, vol. 67, no. 12, pp. 5031–5039, Dec. 2020.

[7] P. Li, H. Ren, and B. Arigong, "A uniplanar 3 × 3 nolen matrix beamformer with beam squint reduction," in *Proc. IEEE Int. Symp. Antennas Propag. North Amer. Radio Sci. Meeting*, Montreal, QC, Canada, Jul. 2020, pp. 515–516.

[8] H. Ren, H. Zhang, Y. Jin, Y. Gu, and B. Arigong, "A novel 2-D 3 × 3 nolen matrix for 2-D beamforming applications," *IEEE Trans. Microw. Theory Techn.*, vol. 67, no. 11, pp. 4622–4631, Nov. 2019.

[9] F. Liu, J. Xu, J.-Y. Pu, J.-H. Su, and L. Zhu, "A hybrid architecture 360° phase shifter with continuously tunable phase shift and low in-band phase error," *IEEE Trans. Microw. Theory Techn.*, vol. 72, no. 8, pp. 4810–4821, Aug. 2024.

[10] X.-Z. Wang, F.-C. Chen, and Q.-X. Chu, "A compact broadband 4×4 Butler matrix with 360° continuous progressive phase shift," *IEEE Trans. Microw. Theory Techn.*, vol. 71, no. 9, pp. 3906–3914, Sep. 2023.

[11] A. Kiyaei, W. Ahmad, S. Zakir, E. M. A. Seragi, A. H. Shah, and S. Zeinolabedinzadeh, "Interference-tolerant wireless distributed beamforming receiver array with low-latency frequency synchronization," *IEEE Trans. Microw. Theory Techn.*, vol. 73, no. 7, pp. 3893–3906, Jul. 2025.

[12] R. Rotman, M. Tur, and L. Yaron, "True time delay in phased arrays," *Proc. IEEE*, vol. 104, no. 3, pp. 504–518, Mar. 2016.

[13] V. Boljanovic et al., "Fast beam training with true-time-delay arrays in wideband millimeter-wave systems," *IEEE Trans. Circuits Syst. I, Reg. Papers*, vol. 68, no. 4, pp. 1727–1739, Apr. 2021.

[14] S. K. Garakoui, E. A. M. Klumperink, B. Nauta, and F. E. van Vliet, "Compact cascadable gm-C all-pass true time delay cell with reduced delay variation over frequency," *IEEE J. Solid-State Circuits*, vol. 50, no. 3, pp. 693–703, Mar. 2015.

[15] X. G. Huang and S. Y. Chen, "A 5ps resolution, 5-bit true time delay chip for wideband RF self-interference cancellation," in *Proc. Int. Conf. Microw. Millim. Wave Technol. (ICMMT)*, Qingdao, China, May 2023, pp. 1–3.

[16] S. R. Aghazadeh, H. Martinez, and A. Saberkari, "5 GHz CMOS all-pass filter-based true time delay cell," *Electronics*, vol. 8, no. 1, p. 16, Dec. 2018.

[17] Y. Guo et al., "A true-time-delay transmit/receive module for X-band subarray phased arrays," *IEICE Electron. Exp.*, vol. 14, no. 22, 2017, Art. no. 20171039.

[18] D. I. Lialios, N. Ntetsikas, K. D. Paschaloudis, C. L. Zekios, S. V. Georgakopoulos, and G. A. Kyriacou, "Design of true time delay millimeter wave beamformers for 5G multibeam phased arrays," *Electronics*, vol. 9, no. 8, p. 1331, Aug. 2020.

[19] C.-C. Shen and P.-Y. Hsieh, "Low-complexity delay-multiply-and-sum (DMAS)beamforming using baseband spatial coherence," in *Proc. IEEE Int. Ultrason. Symp. (IUS)*, Kobe, Japan, Oct. 2018, pp. 1–9.

[20] S. Xu et al., "Optical beamforming system based on polarization manipulation with amplitude-phase coupling suppression," *IEEE Trans. Microw. Theory Techn.*, vol. 71, no. 5, pp. 2215–2221, May 2023.

[21] L. Jin, M. Ru, X. Xie, Y. Zhang, and J. Xue, "A novel optically controlled BeamForming network using fiber Bragg gratings," *IEEE Photon. Technol. Lett.*, vol. 36, no. 8, pp. 547–550, Apr. 15, 2024.

[22] Y. Liu, J. Yang, and J. Yao, "Continuous true-time-delay beamforming for phased array antenna using a tunable chirped fiber grating delay line," *IEEE Photon. Technol. Lett.*, vol. 14, no. 8, pp. 1172–1174, Aug. 2002.

[23] Q. Zhang et al., "Two-dimensional phased-array receiver based on integrated silicon true time delay lines," *IEEE Trans. Microw. Theory Techn.*, vol. 71, no. 3, pp. 1251–1261, Mar. 2023.

[24] H. Zhang and B. Arigong, "A novel frequency reconfigurable RF Hilbert transformer for real-time analog signal processing," *IEEE Trans. Circuits Syst. II, Exp. Briefs*, vol. 70, no. 4, pp. 1361–1365, Apr. 2023.

[25] R. Islam, M. H. Maktoomi, H. Ren, and B. Arigong, "Spectrum aggregation dual-band real-time RF/microwave analog signal processing from microstrip line high-frequency Hilbert transformer," *IEEE Trans. Microw. Theory Techn.*, vol. 69, no. 11, pp. 4647–4657, Nov. 2021.

[26] H. Ren, M. Zhou, Y. Gu, and B. Arigong, "A tunable transmission line with controllable phase shifting and characteristic impedance," *IEEE Trans. Circuits Syst. II, Exp. Briefs*, vol. 67, no. 10, pp. 1720–1724, Oct. 2020.

Muhammad Uzair (Graduate Student Member, IEEE) was born in Khyber Pakhtunkhwa, Pakistan, in 2000. He received the B.S. degree in electrical engineering from the National University of Sciences and Technology (NUST), Islamabad, Pakistan, in 2023. He is currently pursuing the Ph.D. degree in electrical engineering at Florida A&M University—Florida State University (FAMU-FSU) College of Engineering, Tallahassee, FL, USA.

During his undergraduate studies, he was actively involved in research and internships at the Research Institute for Microwave and Millimeter Wave Studies (RIMMS), Islamabad. Following graduation, he joined RWR (Pvt.) Ltd., Islamabad, as a Design Engineer with the RF and Microwave Department, where he gained over a year of industry experience. In 2024, he began working as a Research Assistant at Florida A&M University—Florida State University (FAMU-FSU) College of Engineering. His current research focuses on RF circuits and systems, with interests spanning RF transceivers, active and passive components, MMICs, communication systems, and mmWave radars.

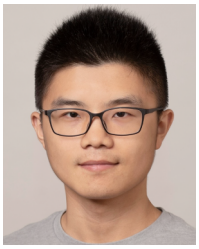

Hanxiang Zhang (Graduate Student Member, IEEE) was born in Yangzhou, China. He received the B.S. degree in electrical engineering from Huaiyin Normal University, Huaian, China, in 2016, the dual M.S. degree in electrical engineering from Washington State University, Vancouver, WA, USA, in 2019, and the University of Notre Dame, South Bend, IN, USA, in 2021, and the Ph.D. degree in electrical engineering from Florida State University, Tallahassee, FL, USA, in 2025.

He is currently a Post-Doctoral Research Scholar at Florida A&M University—Florida State University (FAMU-FSU) College of Engineering. His research interests include RF/microwave and mmWave circuit design, RF antenna, electromagnetic device, beamforming phased array, radar sensing system, wideband beamforming RF transceiver system, and real-time RF/analog signal processing.

Ayesha Naseem (Student Member, IEEE) was born in Punjab, Pakistan, in 2003. She received the B.S. degree in electrical engineering from the National University of Sciences and Technology (NUST), Islamabad, where she was actively engaged in undergraduate research and internship at the Microwave Engineering Research Lab (MERL). She is currently pursuing the Ph.D. degree in electrical engineering at Florida A&M University—Florida State University (FAMU-FSU) College of Engineering, Tallahassee, FL, USA.

After graduation, she joined RWR (Pvt.) Ltd., Islamabad, Pakistan, as an RF/Microwave Design Engineer. She is currently a Research Assistant at Florida A&M University—Florida State University (FAMU-FSU) College of Engineering. Her interests include MMIC design, passive RF/microwave circuits, and beamforming networks for advanced communication and sensing systems.

Bayaner Arigong (Senior Member, IEEE) was born in Inner Mongolia, China. He received the B.Sc. and M.Sc. degrees from China University of Geosciences (CUG), Wuhan, China, in 2005 and 2008, respectively, and the Ph.D. degree in computer science and engineering from the University of North Texas, Denton, TX, USA, in 2015.

He is currently an Associate Professor with the Department of Electrical and Computer Engineering, Florida A&M University—Florida State University College of Engineering, Tallahassee, FL, USA. His research interests include RF/Microwave signal processing circuits, beamforming phased array, 3-D printing RF circuits and system integration, RF power amplifier, quantum microwave chip, electromagnetic device, transformation optics, and nano-photonics.

Dr. Arigong has been in Technical Program Committees and session chairs in IEEE conferences as the IEEE International Microwave Symposium (IMS), Radio and Wireless Week (RWW), European Conferences on Antenna and Propagation (EuCAP), IEEE Wireless and Microwave Technology Conference (WAMICON), and IEEE AP-S Antennas and Propagation Symposium.